JACS
JOURNAL OF THE AMERICAN CHEMICAL SOCIETY
Communication
pubs.acs.org/JACS

Neighboring-Cation Substitution Tuning of Photoluminescence by Remote-Controlled Activator in Phosphor Lattice

Siao-Shan Wang,[†,#] Wei-Ting Chen,[†,#] Ye Li,[‡] Jing Wang,[‡] Hwo-Shuenn Sheu,[§] and Ru-Shi Liu*[,†]

[†]Department of Chemistry, National Taiwan University, Taipei 106, Taiwan

[‡]MOE Key Laboratory of Bioinorganic and Synthetic Chemistry, State Key Laboratory of Optoelectronic Materials and Technologies, School of Chemistry and Chemical Engineering, Sun Yat-sen University, Guangzhou, Guangdong 510275, China

[§]National Synchrotron Radiation Research Center, Hsinchu 300, Taiwan

Supporting Information

ABSTRACT: Highly efficient red phosphors with superior intrinsic properties that are excited by ultraviolet or blue light-emitting diodes are important white light sources for our daily life. Nitride-based phosphors, such as $Sr_2Si_5N_8$:Eu^{2+} and $CaAlSiN_3$:Eu^{2+}, are commonly more red-shifted in photoluminescence and have better thermal/chemical stability than oxides. Cation substitutions are usually performed to optimize photoluminescence and thermal quenching behavior. However, the underlying mechanisms are unclear in most cases. Here we show that neighboring-cation substitution systematically controls temperature-dependent photoluminescence behavior in $CaAlSiN_3$:Eu^{2+} lattice. Trivalent cation substitution at the Ca^{2+} site degrades the photoluminescence in high-temperature environments but achieves better thermal stability when the substituted cation turns monovalent. The neighboring-cation control of lifetime decay is also observed. A remote control effect that guides Eu^{2+} activators in selective Ca^{2+} sites is proposed for neighboring-cation substitution while the compositional Si^{4+}/Al^{3+} ratio adjusts to the valence of M^{n+} (n = 1−3) cation. In the remote control effect, the Eu^{2+} activators are surrounded with nitride anions which neighbor with M^{3+}-dominant and Si^{4+}/Al^{3+}-equivalent coordination when M is trivalent, but shift to the site where surrounded nitride anions neighbor with M^{+}-dominant and Si-rich coordination when M is monovalent. This mechanism can efficiently tune optical properties, especially thermal stability, and could be general to luminescent materials, which are sensitive to valence variation in local environments.

Nitridosilicate materials are widely used as red phosphors for white light-emitting diodes (LEDs) because of their high quantum efficiency and low thermal quenching behavior.[1−9] Many studies have investigated synthetic approaches and structural analysis for $CaAlSiN_3$ phosphor materials.[10−16] However, a cation substitution effect that systematically tunes thermal quenching behavior by controlling the activator sites is scarcely reported. The materials which are made by substituting La^{3+}/Al^{3+} for Ca^{2+}/Si^{4+} and Li^{+}/Si^{4+} for Ca^{2+}/Al^{3+} in $CaAlSiN_3$:Eu^{2+} lattice with a constant 0.5% Eu^{2+} dopant at the Ca^{2+} site to create $(Ca_{1-x}La_x)(Al_{1+x}Si_{1-x})N_3$:Eu (La series) and $(Ca_{1-x}Li_x)(Al_{1-x}Si_{1+x})N_3$:Eu (Li series) solid solutions, respectively, were prepared and characterized in this study.

Linear shifts in the lattice parameters in both series, which are represented by increasing x, are plotted in Figure 1a.

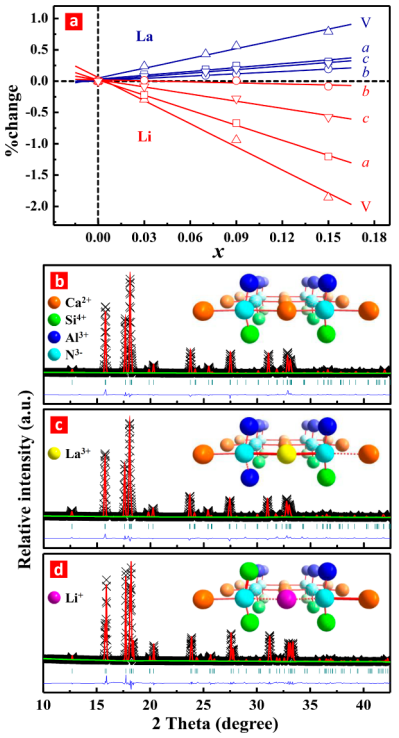

Figure 1. Structural results for La and Li series materials. (a) Relative changes in the lattice parameters with x. (b−d) X-ray Rietveld refinements for (b) $CaAlSiN_3$:Eu, (c) $(Ca_{1-x}La_x)(Al_{1+x}Si_{1-x})N_3$:Eu, and (d) $(Ca_{1-x}Li_x)(Al_{1-x}Si_{1+x})N_3$:Eu ($x$ = 0.15).

However, each kind of lattice parameter in the two series diverges with x, and the peaks of the synchrotron X-ray diffraction patterns also shift to opposite directions, as shown in Figure S1 (Supporting Information).

This result demonstrates that solid solutions are formed in both materials. Figure 1b−d presents the X-ray Rietveld

Received: May 6, 2013
Published: August 13, 2013

   dx.doi.org/10.1021/ja404510v | J. Am. Chem. Soc. 2013, 135, 12504−12507

refinement results of the $CaAlSiN_3$:Eu material (x = 0.00 sample), as well as those of the La and Li series at x = 0.15. The local environments of the corresponding crystal structures are shown in the insets of Figure 1b–d. The sum of the ionic radii of the $CaAlSiN_3$ parent structure [$^{[6]}r(Ca^{2+})$ + $^{[4]}r(Al^{3+})$ + $^{[4]}r(Si^{4+})$ = 1.00 + 0.39 + 0.26 = 1.65 Å] is smaller than that of the La lattice [$^{[6]}r(La^{3+})$ + $^{[4]}r(Al^{3+})$ + $^{[4]}r(Al^{3+})$ = 1.032 + 0.39 + 0.39 = 1.812 Å], but larger than that of the Li lattice [$^{[6]}r(Li^{+})$ + $^{[4]}r(Si^{4+})$ + $^{[4]}r(Si^{4+})$ = 0.76 + 0.26 + 0.26 = 1.28 Å].[17] Therefore, the lattice expansion with x in the La series materials is attributed to the cation substitution of Ca^{2+}/Si^{4+} by La^{3+}/Al^{3+}. By contrast, a contraction in the Li series is observed in the substitution of Ca^{2+}/Al^{3+} by Li^{+}/Si^{4+}. The relative change in the sum of the ionic radii in both series [(1.812 − 1.65)/(1.65 − 1.28) = 45.9%] is closely consistent with the relative change in volume (Figure 1a shows that the % changes in the La and Li series are +0.83 and −1.79, respectively, when x = 0.15; 0.83/1.79 = 46.4%). This result indicates that the La^{3+}/Al^{3+} and Li^{+}/Si^{4+} pairs are introduced into the $CaAlSiN_3$ lattice.

The photoluminescence excitation and emission spectra of both series are shown in Figure 2. The maximum emission peak

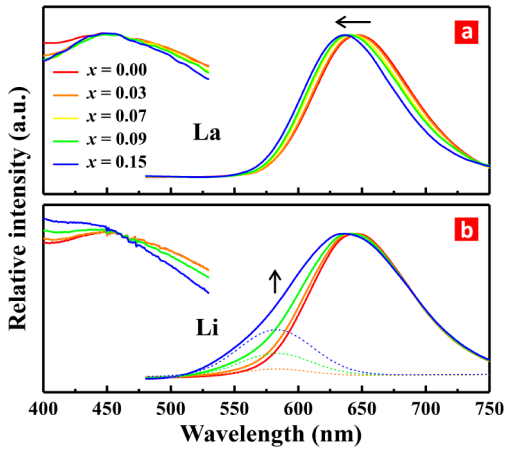

Figure 2. Photoluminescence excitation and emission spectra of (a) $(Ca_{1-x}La_x)(Al_{1+x}Si_{1-x})N_3$:Eu and (b) $(Ca_{1-x}Li_x)(Al_{1-x}Si_{1+x})N_3$:Eu. The photoluminescence spectra are obtained upon excitation by 460 nm light. The arrows present the energy shift for the emission spectra of the La series and the relative intensity change for the Li series with increasing x. The photoluminescence spectra of the Li series are decomposed into two Gaussian peaks from different Eu^{2+} environments. Details of the two decomposed peaks are depicted in Figure S2.

in the La series is influenced by the lattice structure and shifts to a shorter wavelength region with x. This energy shift in the photoluminescence might be attributed to a decrease in the crystal field splitting of 5d orbitals caused by lattice expansion. However, an unexpected result is observed in the photoluminescence spectra of the Li series. The full width at half-maximum of the emission peak progressively broadens with increasing x rather than shifting to a longer wavelength region despite the lattice contraction in the Li series. The emission spectra of the Li series can therefore be fitted into two Gaussian contributions as shown in Figure S2, suggesting that the photoluminescence property is significantly correlated with the local environment of activators.

The thermal stability is important in ensuring a high efficiency of phosphor-converted devices.[3,18−21] Figures 3a,b show temperature-dependent photoluminescence spectra for

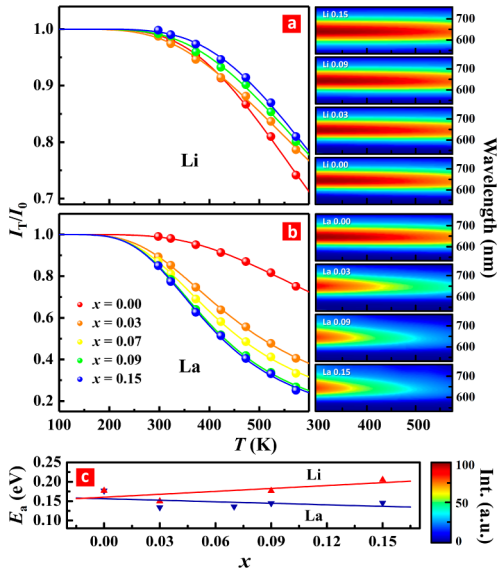

Figure 3. Thermal quenching behavior of photoluminescence for (a) $(Ca_{1-x}Li_x)(Al_{1-x}Si_{1+x})N_3$:Eu and (b) $(Ca_{1-x}La_x)(Al_{1+x}Si_{1-x})N_3$:Eu samples. Temperature-dependent photoluminescence spectra are shown in the right-hand side. These curves are fitted by $I_T/I_0 = [1 + D\exp(-E_a/kT)]^{-1}$, where I_0 (intensity at T = 0), D, and activation energy E_a are refined variables. (c) Plot of activation energies with variable x for La and Li series.

both series. The thermal quenching behavior of photoluminescence is measured from ambient temperature to 573 K. The emission intensities (I_T) of all samples decrease with increasing environmental temperature, as demonstrated at the right-hand side of Figure 3. The emission intensity of the parent $CaAlSiN_3$:Eu material (x = 0.00) decreases faster than that in the Li series with increasing temperature, but much slower than that in the La series. The overall trend of thermal quenching behavior progressively improves across the overall samples from the La series (x = 0.15 to 0.03) to the intermediate x = 0.00 sample, and then to the Li series (x = 0.03 to 0.15). This result is unusual and illustrates an opposite phenomenon against covalence balance among entire cations and nitride anions, in which the $CaSi^{6+}$ and $CaAl^{5+}$ cation pairs are substituted by $LaAl^{6+}$ and $LiSi^{5+}$ pairs, respectively, to compensate the covalence change, as the quenching activation barriers of both series samples should be consistent with unsubstituted x = 0.00 sample. Both trends in the photoluminescence and thermal quenching behavior reflect that the Eu^{2+} activators are sensitive to the local sites, which are connected with the nearest nitride anions and other cation neighbors.

In order to examine virtually the interaction between a doping element and the surrounding anion coordination, La L_3-edge extended X-ray absorption fine structure spectroscopy is employed to analyze specific local bonding in this study. The nearest bond distances of the La^{3+} cations and the surrounding N^{3-} anions are shown in Figure S3. The average La–N distances (d_{La-N} = 2.18–2.27 Å with composition variable x) of the La series materials are shorter than the average Ca–N bond distance (d_{Ca-N} = 2.51 Å, calculated from the X-ray Rietveld refinement) of the $CaAlSiN_3$:Eu sample. This condition is caused by the larger valence of La^{3+} cation than the Ca^{2+} cation. Thus, the nitride anion connecting with a La^{3+} cation would introduce more covalence than with a Ca^{2+} cation, suggesting

dx.doi.org/10.1021/ja404510v | J. Am. Chem. Soc. 2013, 135, 12504–12507

that the binding strength of La−N is stronger than that of Ca−N. Conversely, the binding strength of Li−N is theoretically weaker than that of Ca−N because of a relatively weak covalent interaction between the Li^+ cation and the nitride anion. Hence, a possible mechanism in which the accommodation of the Eu^{2+} activator is controlled by covalent variable neighboring cations is proposed to elucidate the variations in the photoluminescence and quenching behavior in both series as follows.

The central Ca^{2+} cation is surrounded by coordinated nitrides that also have other branches connecting with neighboring cations, e.g., Si^{4+}, Al^{3+}, and outer Ca^{2+} cations. The central Ca^{2+} cation is substituted by a La^{3+} cation with increasing x, $LaAl^{6+}$ pair, in the La series, while the neighboring Si^{4+} cation at the second shell is substituted by Al^{3+}. In the Li series, the central Ca^{2+} cation is substituted by a Li^+ cation with x, $LiSi^{5+}$ pair, while the neighboring Al^{3+} cation at the second shell is substituted by Si^{4+}. Systematical models for neighboring-cation substitutions are shown in Figure 4. Therefore, this model controls the accommodation of Eu^{2+} activators in both series, as presented in Figure 4b,c.

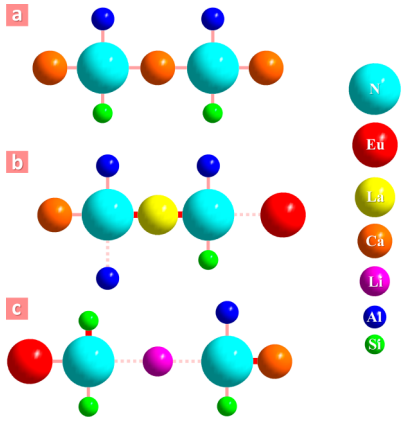

Figure 4. Local structural coordination of (a) $CaAlSiN_3$, (b) La, and (c) Li series lattices. The remote-controlled mechanism for Eu^{2+} activators at selected Ca^{2+} sites is proposed for neighboring-cation substitutions. The dashed line represents the longer and looser bond. The broad solid line represents the shorter and tenser bond.

The covalence of La−N and Li−N competes with the bonding of the nitride anions to other neighboring cations. In the La series, La−N is more covalent than the outer Ca−N when the $LaAl^{6+}$ pair is introduced, reflecting a tenser and shorter La−N than the original unsubstituted Ca−N of the x = 0.00 sample, but essentially gaining a longer and looser outer Ca−N. With the introduction of the La^{3+} cation at the central site, the Al^{3+} cation simultaneously substitutes in the Si^{4+} site, which results in an emergence of two different outer Ca^{2+} sites. These two covalence-dependent Ca^{2+} sites are attributed to two different nitrides' coordination linking with the $AlAl^{6+}$ or $AlSi^{7+}$ pair. The Al^{3+} cation substitution for the Si^{4+} site would also lead to a longer and looser Al−N compared with the original unsubstituted Si−N of the x = 0.00 sample. The degree of valence in the bonding of the nitride, connecting with La^{3+} and two Al^{3+} cations, to the outer Ca^{2+} cation is compensated, as well as the Ca−N of the x = 0.00 sample. The bonding of the other nitride, connecting with the La^{3+} cation and $AlSi^{7+}$ pair, to the outer Ca^{2+} cation is relatively longer. As Eu^{2+} activator is introduced, it would preferably be accommodated at the looser Ca^{2+} site to minimize the lattice strain because the Eu^{2+} cation ($^{[6]}r(Eu^{2+})$ = 1.17 Å) is larger than the Ca^{2+} cation ($^{[6]}r(Ca^{2+})$ = 1.00 Å).[17] Therefore, the selective accommodation for the Eu^{2+} activator in the La series is determined by the bonding of the nitride connecting to the La^{3+} cation and the $AlSi^{7+}$ pair, thereby providing a weak covalent coordination environment for the Eu^{2+} activator.

A reverse argument applies to predict the Eu^{2+} activator accommodation in the Li series. Here Li−N is looser and the outer Ca−N is tenser, but the degree of covalence in one kind of outer Ca−N is compensated, as well as the original Ca−N. Therefore, the Eu^{2+} activator is controlled to locate at the relatively loose outer Ca^{2+} site, which is connected to the nitride with Li^+ cation and $SiSi^{8+}$ pair branches—namely, the Si-rich site.

The proposed model for both photoluminescence and quenching properties is observed, and the mechanism of local environmental variation is evidenced below. The Eu^{2+} activators in both series accommodate at the relatively loose site (the lattice stain is minimized for different atomic sizes). Thus, the photoluminescence in the La series is expected to blue shift because the Eu^{2+} accommodations progressively decrease in the covalent character and crystal field strength with x. By contrast, the surrounding nitrides of Eu^{2+} activators in the Li series connect with excess Si^{4+} neighbors, which give rise to a smaller centroid shift than that with Si^{4+}/Al^{3+}-equivalent neighbors for Eu^{2+} activators.[22] This result creates the other high-energy emission as fitted in Figure S2, in agreement with that found in the previous literature.[14] Detailed Si^{4+} environmental analysis is performed via solid-state NMR spectroscopy as shown in Figures S4 and S5. The result demonstrates that the Si^{4+}/Al^{3+} ratio is tuned through the substitution process.

Excited electrons of activator in a high-temperature environment easily cross the activation barrier and release energy by a quenching process when the binding of the activator to the coordinated anions is weak (essentially a condition of facile vibrational energy transfer in soft structure). In this study, the thermal stability of La series materials worsens because the covalence of Eu−N herein decreases as x increases, which results in a low activation barrier and significant thermal quenching. The thermal quenching rate of the Li series should be theoretically similar to that of the x = 0.00 sample because the Eu^{2+} activator accommodation is nearly consistent with the original Ca^{2+} site, as previously demonstrated. However, a surprising phenomenon is observed, in which the quenching behavior practically improves, suggesting that the binding strength of Eu−N is slightly stronger and tighter when $LiSi^{5+}$ substitutions are introduced. A quantitative calculation is roughly estimated as follows: the Eu^{2+} activators are coordinated with nitride anions linking with Li^+ and two Si^{4+} (original and substituted Si^{4+}) cations, where a covalence competition occurs between the Li^+ and the substituted Si^{4+} cations for the nitride electron cloud. The Li^+−N^{3-} bonding is 50% looser compared with the original Ca^{2+}−N^{3-} bonding [$(Q_{Li} - Q_{Ca})/Q_{Ca}$ = [(1+) − (2+)]/(2+) = −50% change], but the Si^{4+}−N^{3-} bonding is 33% tenser compared with the Al^{3+}−N^{3-} bonding [$(Q_{Si}-Q_{Al})/Q_{Al}$ = [(4+) − (3+)]/(3+) = 33% change]. Hence, a complementary result gives rise to a slightly tighter Eu−N in the Li series than that in the parent $CaAlSiN_3$:Eu material, leading to a higher quenching activation barrier. On the other hand, the reverse result is obtained in the La series, as previously mentioned. The valence change in the neighboring-cation substitutions for entire lattices is balanced, but a local covalence-driven influence for Eu^{2+} activators drives

dx.doi.org/10.1021/ja404510v | J. Am. Chem. Soc. 2013, 135, 12504−12507

a systematic change in the quenching behavior for the La series, x = 0.00, and Li series materials.

The above covalence-driven influence also accounts for the remote-controlled Eu^{2+} activators of decay profiles as shown in Figure 5. The binding strength between activator and

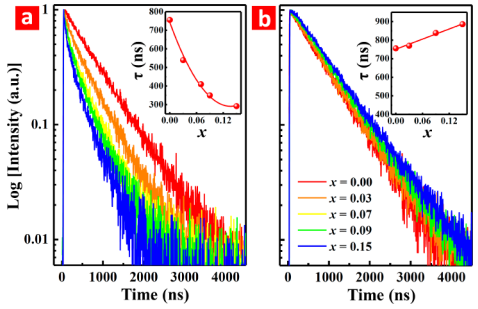

Figure 5. Luminescence of decay profiles for (a) $(Ca_{1-x}La_x)(Al_{1+x}Si_{1-x})N_3$:Eu and (b) $(Ca_{1-x}Li_x)(Al_{1-x}Si_{1+x})N_3$:Eu. All materials are excited at a wavelength of 460 nm at ambient temperature. The insets show plots of the fitted lifetimes (τ) against x for both series.

coordinated nitride anions also influences the photoluminescence lifetime through nonradiative relaxation, such as multiphonon decay or energy transfer from activators to the other neighbors.[23] The lifetime slightly increases in the Li series with x, but rapidly decreases in the La series. This trend coincides with the thermal quenching behavior. This remote control effect demonstrates the site selectivity for activators in the photoluminescence and also controls the nonradiative processes such as thermal quenching and photoluminescence decay behaviors.

In summary, the remote control effect for activators disclosed from $CaAlSiN_3$ material could be used to tune photoluminescence, thermal quenching, and lifetime decay properties in related neighboring-cation-substituted phosphors. This effect may help reveal the underlying mechanisms in optical changes by adjusting the cation/anion composition of phosphors. In addition, the cation substitution influence would be expected to be general not only to luminescent materials but to other functional materials, which are sensitive to valence change at specific sites. For instance, cation substitution-driven valence variation might be crucial to $AA'_3B_4O_{12}$ perovskite-type solid solutions in A-site-ordered $Na^{+}Mn^{2.33+}{}_3V^{4+}{}_4O_{12}$–$Ca^{2+}Mn^{2+}{}_3V^{4+}{}_4O_{12}$–$La^{3+}Mn^{2+}{}_3V^{3.75+}{}_4O_{12}$ and A′-B intersite charge transfer $La^{3+}Cu^{2+}{}_3Fe^{3.75+}{}_4O_{12}$–$Bi^{3+}Cu^{3+}{}_3Fe^{3+}{}_4O_{12}$ magnetic ceramics.[24,25]

■ ASSOCIATED CONTENT

Ⓢ Supporting Information

Experimental methods and supporting tables and figures. This material is available free of charge via the Internet at http://pubs.acs.org.

■ AUTHOR INFORMATION

Corresponding Author

rsliu@ntu.edu.tw

Author Contributions

#S.-S.W. and W.-T.C. contributed equally to this work.

Notes

The authors declare no competing financial interest.

■ ACKNOWLEDGMENTS

This work was supported by the National Science Council of the Republic of China, Taiwan (Contract No. NSC 101-2113-M-002-014-MY3).

■ REFERENCES

(1) Hoppe, H. A. *Angew. Chem., Int. Ed.* **2009**, *48*, 3572.
(2) Zeuner, M.; Pagano, S.; Schnick, W. *Angew. Chem., Int. Ed.* **2011**, *50*, 7754.
(3) Chen, W. T.; Sheu, H. S.; Liu, R. S.; Attfield, J. P. *J. Am. Chem. Soc.* **2012**, *134*, 8022.
(4) Yeh, C. W.; Chen, W. T; Liu, R. S.; Hu, S. F.; Sheu, H. S.; Chen, J. M.; Hintzen, H. T. *J. Am. Chem. Soc.* **2012**, *134*, 14108.
(5) Xie, R. J.; Hirosaki, N. *Sci. Technol. Adv. Mater.* **2007**, *8*, 588.
(6) Xie, R. J.; Hirosaki, N.; Li, Y.; Takeda, T. *Materials* **2010**, *3*, 3777.
(7) He, X. H.; Lian, N.; Sun, J. H.; Guan, M. Y. *J. Mater. Sci.* **2009**, *44*, 4763.
(8) Yang, S. H.; Lin, J. S.; Juang, F. S.; Chou, D. C.; Chung, M. H.; Chen, C. M.; Liu, L. C. *Curr. Appl. Phys.* **2013**, *13*, 931.
(9) Brinkley, S. E.; Pfaff, N.; Denault, K. A.; Zhang, Z. J.; Hintzen, H. T.; Seshadri, R.; Nakamura, S.; DenBaars, S. P. *Appl. Phys. Lett.* **2011**, *99*, 241106.
(10) Li, J.; Watanabe, T.; Wada, H.; Setoyama, T.; Yoshimura, M. *Chem. Mater.* **2007**, *19*, 3592.
(11) Piao, X.; Machida, K. I.; Horikawa, T.; Hanzawa, H.; Shimomura, Y.; Kijima, N. *Chem. Mater.* **2007**, *19*, 4592.
(12) Li, J.; Watanabe, T.; Sakamoto, N.; Wada, H.; Setoyama, T.; Yoshimura, M. *Chem. Mater.* **2008**, *20*, 2095.
(13) Li, Y. Q.; Hirosaki, N.; Xie, R. J.; Takeda, T.; Mitomo, M. *Chem. Mater.* **2008**, *20*, 6704.
(14) Jung, Y. W.; Lee, B.; Singh, S. P.; Sohn, K. S. *Opt. Exp.* **2010**, *18*, 17805.
(15) Uheda, K.; Hirosaki, N.; Yamamoto, Y.; Naito, A.; Nakajima, T.; Yamamoto, H. *Electrochem. Solid State Lett.* **2006**, *9*, H22.
(16) Li, Y. Q.; Hirosaki, N.; Xie, R. J.; Takeka, T.; Mitomo, M. *J. Solid State Chem.* **2009**, *182*, 301.
(17) Shannon, R. D. *Acta Crystallogr.* **1976**, *A32*, 751.
(18) Zhang, Z. J.; ten Kate, O. M.; Delsing, A. C. A.; Stevens, M. J. H.; Zhao, J. T.; Notten, P. H. L.; Dorenbos, P.; Hintzen, H. T. *J. Mater. Chem.* **2012**, *22*, 23871.
(19) Zhang, Z. J.; ten Kate, O. M.; Delsing, A.; van der Kolk, E.; Notten, P. H. L.; Dorenbos, P.; Zhao, J. T.; Hintzen, H. T. *J. Mater. Chem.* **2012**, *22*, 9813.
(20) Ronda, C. R. *Luminescence: From Theory to Applications*; Wiley-VCH Verlag GmbH & Co. KGaA: Weinheim, 2008.
(21) Shigeo, S.; William, M. *Phosphor Handbook*; CRC Press: Washington, DC, 1998.
(22) Dorenbos, P. *Phys. Rev. B* **2001**, *64*, 125117.
(23) Layne, C. B.; Lowdermilk, W. H.; Weber, M. J. *Phys. Rev. B* **1977**, *16*, 10.
(24) Zhang, S.; Saito, T.; Mizumaki, M.; Chen, W. T.; Tohyama, T.; Shimakawa, Y. *J. Am. Chem. Soc.* **2013**, *135*, 6056.
(25) Long, Y. W.; Hayashi, N.; Saito, T.; Azuma, M.; Muranaka, S.; Shimakawa, Y. *Nature* **2009**, *458*, 60.